

Quantum anomalous Hall state in ferromagnetic SrRuO₃ (111) bilayers

Liang Si,¹ Oleg Janson,¹ Gang Li,¹ Zhicheng Zhong,² Zhaoliang Liao,³ Gertjan Koster,³ and Karsten Held¹

¹*Institut für Festkörperphysik, TU Wien, Wiedner Hauptstraße 8-10, 1040 Vienna, Austria*

²*Max-Planck-Institut für Festkörperforschung, Heisenbergstrasse 1, 70569 Stuttgart, Germany*

³*MESA+ Institute for Nanotechnology, University of Twente,
P.O. BOX 217, 7500AE, Enschede, The Netherlands*

(Dated: April 19, 2022)

SrRuO₃ heterostructures grown in the (111) direction are a rare example of thin film ferromagnets. By means of density functional theory plus dynamical mean field theory we show that the half-metallic ferromagnetic state with an ordered magnetic moment of $2\mu_B/\text{Ru}$ survives the ultimate dimensional confinement down to a bilayer, even at elevated temperatures of 500 K. In the minority channel, the spin-orbit coupling opens a gap at the linear band crossing corresponding to $\frac{3}{4}$ filling of the t_{2g} shell. We demonstrate that the respective state is Haldane's quantum anomalous Hall state with Chern number $C=1$, without an external magnetic field or magnetic impurities.

The discovery of topological states of matter [1–3] has significantly broadened and advanced our understanding of solid state physics. The historically first topological phenomenon is the quantum Hall effect [4] (QHE) observed in a two-dimensional electronic system exposed to a strong external magnetic field. The QHE manifests itself in the quantized transverse conductance (Hall conductance) stemming from nontrivial Berry curvatures of the filled Landau levels [5–7] in an otherwise insulating state with a vanishing longitudinal conductance. As a result, a dissipationless edge mode appears along the boundary between the quantum Hall system and the vacuum.

In his Nobel prize winning work, Haldane [8] realized that neither magnetic field nor Landau levels are actually required, but only breaking of time-reversal symmetry (TRS) and a non-trivial topology of the electronic structure. Arguably the easiest way to break TRS without magnetic field is through a spontaneous magnetization, inducing a quantized version of the conventional anomalous Hall effect, which is now known as the quantum anomalous Hall effect (QAH). Such insulating bulk systems are also called Chern insulators, as their topological edge states are characterized by the first Chern number, which is defined as an integral of the Berry curvature of the filled bands over the Brillouin zone.

Recent research on quantum spin-Hall (QSH) insulators [9–11], which can be viewed as two copies of a QAH state with equal but opposite magnetic moments, delivered an impressive number of candidate materials. In contrast, the search of QAH systems is far from being comprehensive owing to the strict conditions for realizing them, *i.e.*, realizing the spontaneous magnetization and the nontrivial Berry curvatures. One straightforward route is to magnetically dope a QSH insulator, where the presence of the magnetic impurity breaks the TRS and, thus, lifts the Kramers degeneracy of the QSH insulators to reach the QAH states [12, 13]. However, experimentally such extrinsic impurities are difficult to control, and need to generate a sufficiently strong magnetic

moment while keeping the topology of the system unaffected. Thus, it is of more fundamental interest to have a genuine magnetic system that hosts the QAH state intrinsically.

In this context, heterostructures of transition-metal oxides (TMO) are a most promising material class. These artificial materials exhibit a plethora of interesting behaviors driven by electronic correlations and the dimensional confinement [14–17]. Grown perpendicular to the body diagonal of a perovskite lattice structure, *i.e.* along the [111] direction, bilayers of perovskite TMO form a honeycomb lattice. The d -electrons in such bilayers can show a fascinating variety of electronic, magnetic as well as topological [18] phases. Some heterostructures such as LaAuO₃-LaCrO₃ heterostructures were suggested as a realization of the QAH state [19]. However, the fabrication of such heterostructures is at best challenging, because bulk LaAuO₃ is not of the perovskite structure [20]. Also freestanding monolayers of e.g. NiCl₃ have also been proposed [21, 22]. Against this background, actual material realizations of Haldane's QAH state remain a great challenge.

In this letter, we investigate the electronic structure of (111)-oriented SrRuO₃ (SRO) bilayers sandwiched between SrTiO₃ (STO). This heterostructure can be routinely fabricated by advanced pulsed laser [23] or metal-organic aerosol [24] deposition, and thin SRO (111) films already exist and are ferromagnetic [25–28]. Using density functional theory (DFT) and dynamical mean field theory (DMFT) calculations, we show that SRO (111) bilayers remain ferromagnetic half-metals with a moment of $2\mu_B/\text{Ru}$ and a Curie temperature (T_C) exceeding room temperature. The band structure of the minority channel features a linear band crossing at $\frac{3}{4}$ filling of the t_{2g} shell, which becomes gapped due to the spin-orbit coupling (SOC). By simulating the respective microscopic Hamiltonian, we find a QAH state and the Chern number $C = 1$. This result is further corroborated by a direct numerical solution of the full tight-binding Hamiltonian parameterization of the Wannier functions

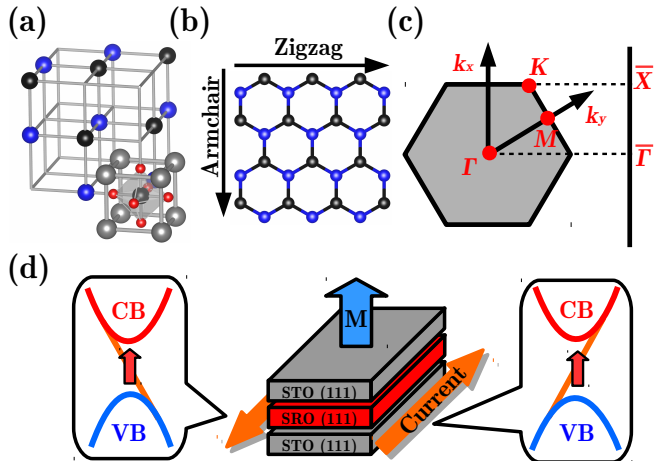


FIG. 1. (Color online) Crystal and electronic structure of 2SRO:7STO (111) superlattices. (a) Octahedral perovskite cage in bulk SrRuO_3 . Gray and red balls denote Sr and O atoms; blue and black ones Ru atoms in two honeycomb sublattices. (b) (111) bilayers of SRO form a honeycomb lattice. (c) High-symmetry points of the first Brillouin zone of the honeycomb lattice: $\Gamma(0,0,0)$, $M(\frac{\pi}{a},0,0)$ and $K(\frac{2\pi}{3a}, \frac{2\pi}{3a}, 0)$. (d) Spin-polarized minority currents develop at the edge of the bilayer, and originate from the topological states between the valence band (VB) and the conduction band (CB) illustrated on the left and right, respectively.

on a long cylinder, which shows topological edge modes in the gap.

Before presenting the results of our DFT+DMFT calculations, we briefly explain how the unit cells are constructed. In the hypothetical cubic perovskite structure of SrRuO_3 [Fig. 1(a)], we consider layers stacked along the body diagonal [111] of the cubic lattice. By cutting out two neighboring SRO monolayers [Fig. 1(b)], we obtain a bilayer whose Ru atoms form a honeycomb lattice. To comply with the periodic boundary conditions and to ensure a sufficient separation of individual SRO bilayers, we interleave them with seven layers of STO. The resulting 2SRO:7STO superlattice with 45 atoms in the unit cell has a pseudocubic structure described within the space group $P\bar{3}m1$ (164) with an inversion center in between the SRO monolayers.

The smaller lattice constant of STO exerts a compressive strain of $\sim 0.45\%$ on the SRO bilayers [29]. To account for strain effects, we relax the c unit cell parameter and the internal atomic coordinates within the generalized gradient approximation (GGA) [30] as implemented in VASP-5.12 [31, 32]. All further electronic structure calculations were performed for this optimized structure using the WIEN2K-14.2 [33] code.

The nonmagnetic GGA band structure of 2SRO:7STO (111) is shown in Fig. 2(a). The manifold crossing the Fermi level comprises six Ru t_{2g} bands. The higher-lying e_g states (not shown) are empty and can be

excluded from the correlated subspace. As a necessary preparatory step for DMFT calculations, we project the Ru t_{2g} bands onto maximally localized Wannier functions [34] using the WIEN2WANNIER code [35].

DMFT calculations were performed using the continuous time quantum Monte Carlo (CT-QMC) solver implemented in the code w2DYNAMICS [36]. The interaction parameters, the Coulomb repulsion $U = 3.0\text{ eV}$ and the Hund's exchange $J = 0.3\text{ eV}$ are adopted from [37]. We use the rotationally invariant form of the Hamiltonian, which implies an inter-orbital interaction $U' = U - 2J$. For the analytical continuation of the resulting self-energy $\Sigma(i\omega_n)$ onto the real frequency axis ω , the maximum entropy method [38] was used.

DMFT reveals strong similarities between 2SRO:7STO (111) superlattices and bulk SrRuO_3 : both are ferromagnetic and conducting in the minority channel. The ferromagnetic half-metallic behavior is in sharp contrast to (001) SRO thin films that are insulators and lack ferromagnetism [37, 39]. This difference stems from the spatial confinement which acts differently in (001) and (111) systems: Slicing in the [001] direction lowers the onsite energy of the xy orbital compared to the xz and yz orbitals [37], favoring antiferromagnetism within the half-filled xz and yz orbitals. In contrast, the degeneracy of the t_{2g} manifold is not affected by (111) slicing, and the on-site orbital energies are similar to bulk SrRuO_3 . And yet, the spatial confinement is important: DMFT indicates that the ferromagnetic state of the 2SRO:7STO (111) superlattice survives up to $\sim 500\text{ K}$ [inset of Fig. 2(b)], which is remarkably higher than the Curie temperature of bulk SRO (160 K). This result is in agreement with recent experimental reports on the enhanced T_C in SRO (111) films [25–28]; and opens a route to long-sought-after ultrathin layers that are ferromagnetic at room temperature. [40]

Next, we evaluate the DMFT self-energy $\Sigma(\omega)$ on the real frequency axis and calculate the k -resolved spectral function $A(k, \omega)$ [Fig. 2(b) and 2(c)]. The effect of the k -independent self-energy is twofold: the real part shifts the bands and renormalizes the band widths, while the imaginary part gives rise to broadening. The latter is particularly for the partially filled majority states: there is a broad incoherent continuum in Fig. 2(b) terminated by a nearly flat feature around 0.2 eV below the Fermi level. In contrast, the k -resolved spectral function for the minority channel [Fig. 2(c)] largely resembles the GGA band structure [Fig. 2(a)]. The most prominent effect of electronic correlations here is the reduction of the band width down to $\sim 0.8\text{ eV}$, which is much smaller than that in the GGA (1.5 eV) and in the bulk SRO (3.2 eV). Altogether the DMFT self energy essentially corresponds to a bandwidth quasiparticle renormalization of $Z \sim 0.5$ and a reduction of the spin-splitting from 0.88 eV in GGA to 0.47 eV in DFT+DMFT; otherwise the electronic structure and its topology is not affected.

A remarkable property of $A(k, \omega)$ in the minority channel is the linear band crossing (at $\frac{3}{4}$ filling of the t_{2g} shell) near the M point and along the Γ -K line. This feature inherited from the band structure [Fig. 2(a)] is resilient to electronic correlations [Fig. 2(c)]. But if the SOC is taken into account a gap opens at the band crossing: the full relativistic treatment within the modified Becke-Johnson (mBJ) potential [41] yields a tiny band gap of ~ 1 meV. Assuming the chemical potential is placed into the gap, the system becomes insulating at low temperatures. Topological properties of this envisaged insulating state are characterized by the Chern number C of the occupied bands: zero or nonzero for a trivial state and the QAH state, respectively.

To determine C , we employ the full tight-binding Hamiltonian parameterization of the Wannier functions. The sizable separation between SRO bilayers allows us to consider only intraplane couplings. The eigenvectors of the respective tight-binding Hamiltonian are calculated on a fine k -mesh of 120×120 points and used to calculate link variables and, in turn, Chern numbers, following the procedure described in Ref. [42]. In this way, we find $C=1$ for the bands below the SOC-induced gap, hence the QAH state is realized.

The Chern number $C=1$ indicates the existence of a topological edge state, or in general, an imbalance of “right moving” and “left moving” edge states by one. To visualize this state, we recast our 2D Hamiltonian into mixed boundary conditions: periodic along one direction and open along the other. The resulting 1D model is solved by using the iterative Green’s function approach [43] to get the spectra on a semi-infinite long cylinder. The band structure (Fig. 3) reveals the presence of edge states of two types: Trivial edge states originate from the conduction [valence] band and rebound back to the conduction [valence] band in Fig. 3(b) [Fig. 3(f)]. In contrast, the topological edge states connect the valence band and the conduction band. The difference in “right moving” (R_n) and “left moving” (L_n) states on each edge further corroborates our Chern number analysis. Please note that the Ru honeycomb in SRO (111) is buckled; Ru atoms at the left and the right edge are at a different height, which explains the left/right asymmetry. Let us also note that for the $C=1$ state, the consideration of the full microscopic model is needed: restricting the model to first-neighbor or first- and second-neighbor couplings only, yields unbalanced topological states as well but with different Chern numbers.

For an experimental observation of edge states, the size of the SOC-induced band gap plays a crucial role. Unfortunately, the gap size in 2 SRO : 7 STO (111) confines the prospective QAH state to low temperatures and impedes its experimental observation. Larger gaps can be obtained by increasing the SOC and/or the trigonal crystal field (Δ_{CF}) splitting. The SOC can vary from several meV to several hundred meV, but requires the substitu-

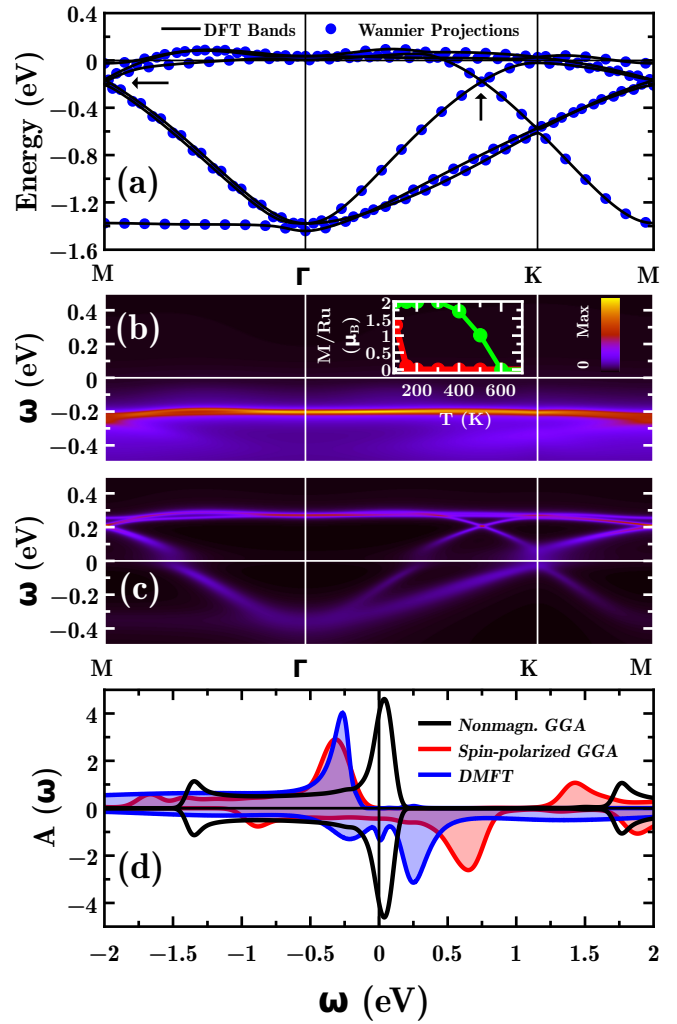


FIG. 2. (Color online) (a) Nonmagnetic scalar relativistic GGA band structure of 2 SRO : 7 STO (solid lines) in comparison with the Fourier-transformed Wannier projections (circles). The arrow indicates the position of the Dirac point near M point and along the Γ -K line. (b) spin-up and (c) spin-down DMFT spectral functions at 300 K. (d) Density of states of nonmagnetic and magnetic GGA calculations in comparison with the DMFT spectral function. Inset in (b): ferromagnetic moment of bulk SRO (red) vs. the SRO (111) bilayer (green) as calculated by DFT+DMFT.

tion of the transition metal. A more sensible approach is to tune Δ_{CF} by choosing a different substrate. But in addition to the change in the gap size, this structural alteration will affect the mutual orientation of RuO_6 octahedron and in turn alter the hopping parameters. Which of the two competing states, the QAH state or the trivial insulator, is eventually stabilized, needs to be pinpointed by a microscopic analysis. Another promising way to enlarge the gap size is electronic doping, which shifts the chemical potential to $\frac{3}{4}$ filling on t_{2g} shell. If the chemical potential is within the gap, we expect an additional enhancement of the gap as e.g. described by the scissor

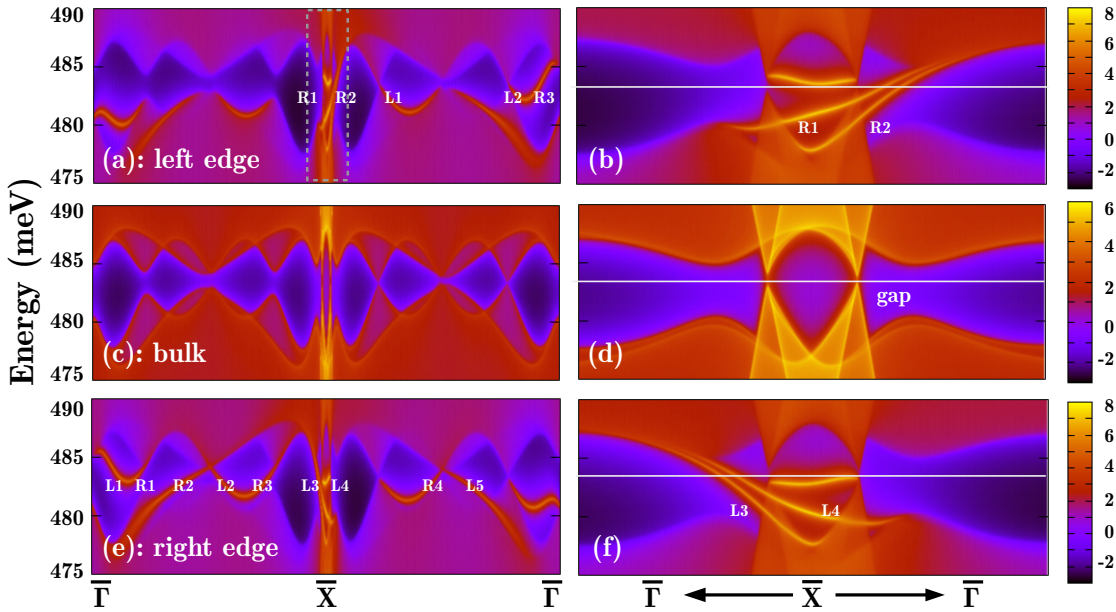


FIG. 3. (Color online) Spectral functions of semi-infinite zigzag-termination slabs of SrRuO₃ (111) bilayers projected in the k_x direction as indicated in Fig. 1. The spectral functions of left edge (a, b), central bulk region (c, d) and right edge (e, f) are shown; the right panels are zoom-ins of the left panels corresponding to the white-dashed box in (a). All edge states are labeled with L_n/R_n ($n=1,2,3\dots$) indicating the n th left/right moving state. Two nearly flat edge states are identified as topological trivial and do not cross the Fermi energy at ~ 483 meV (white solid line). The edge states agree with the Chern number $C = 1$ since e.g. on the left edge (a) there are $3 - 2 = 1$ more right than left “movers”.

operator in GW , see [44] and references therein.

In summary, we have shown that bilayers of SrRuO₃ on a SrTiO₃ substrate in [111] direction emerge to be a candidate of long-sought-after room-temperature ferromagnetic half-metals with an ordered moment of $\sim 2\mu_B$ per Ru. The spin-orbit coupling opens a gap in the unoccupied part of the spectrum, which gives rise to a quantum anomalous Hall (QAH) state with the Chern number $C=1$. Accordingly, a direct simulation of the tight-binding Hamiltonian indicates that the number of left and right movers differs by one. Experimentally, these QAH states can be observed by angular resolved photoemission spectroscopy after laser pumping, as e.g. demonstrated in [45] for other topological surface states.

LS, GL, OJ and KH acknowledge financial support by European Research Council under the European Union’s Seventh Framework Program (FP/2007-2013)/ERC through grant agreement n. 306447. LS also thanks the Austrian Science Fund (FWF) for support through the Doctoral School W1243 Solids4Fun (Building Solids for Function). OJ was supported by the Austrian Science Fund (FWF) through the Lise Meitner programme, project no. M2050. ZZ acknowledges support by the FWF through the SFB ViCoM F4103. ZL acknowledges the financial support from the European Union Council through the 7th Framework Program (FP7) grant nr NMP3-LA-2010-246102 IFOX. GK acknowledges funding from DESCO program of the Dutch Foundation for Fundamental Research on Matter (FOM)

with financial support from the Netherlands Organization for Scientific Research (NWO). We thank A. Sandvik for making available his maximum entropy program. Calculations have been done on the Vienna Scientific Cluster (VSC).

- [1] X.-G. Wen, *Int. J. Mod. Phys. B* **4**, 239 (1990).
- [2] M. Z. Hasan and C. L. Kane, *Rev. Mod. Phys.* **82**, 3045 (2010).
- [3] X.-L. Qi and S.-C. Zhang, *Rev. Mod. Phys.* **83**, 1057 (2011).
- [4] K. v. Klitzing, G. Dorda, and M. Pepper, *Phys. Rev. Lett.* **45**, 494 (1980).
- [5] M. V. Berry, *Proceedings of the Royal Society of London A: Mathematical, Physical and Engineering Sciences* **392**, 45 (1984).
- [6] D. J. Thouless, M. Kohmoto, M. P. Nightingale, and M. den Nijs, *Phys. Rev. Lett.* **49**, 405 (1982).
- [7] D. Xiao, M.-C. Chang, and Q. Niu, *Rev. Mod. Phys.* **82**, 1959 (2010).
- [8] F. D. M. Haldane, *Phys. Rev. Lett.* **61**, 2015 (1988).
- [9] C. L. Kane and E. J. Mele, *Phys. Rev. Lett.* **95**, 146802 (2005).
- [10] M. König, S. Wiedmann, C. Brüne, A. Roth, H. Buhmann, L. W. Molenkamp, X.-L. Qi, and S.-C. Zhang, *Science* **318**, 766 (2007).
- [11] D. Hsieh, D. Qian, L. Wray, Y. Xia, Y. S. Hor, R. J. Cava, and M. Z. Hasan, *Nature (London)* **452**, 970 (2008).
- [12] C.-Z. Chang, J. Zhang, X. Feng, J. Shen, Z. Zhang,

M. Guo, K. Li, Y. Ou, P. Wei, L.-L. Wang, Z.-Q. Ji, Y. Feng, S. Ji, X. Chen, J. Jia, X. Dai, Z. Fang, S.-C. Zhang, K. He, Y. Wang, L. Lu, X.-C. Ma, and Q.-K. Xue, *Science* **340**, 167 (2013).

[13] J. G. Checkelsky, R. Yoshimi, A. Tsukazaki, K. S. Takahashi, Y. Kozuka, J. Falson, M. Kawasaki, and Y. Tokura, *Nat. Phys.* **10**, 731 (2014).

[14] J. Mannhart and D. G. Schlom, *Science* **327**, 1607 (2010).

[15] J. M. Rondinelli and N. A. Spaldin, *Adv. Mater.* **23**, 3363 (2011).

[16] P. Zubko, S. Gariglio, M. Gabay, P. Ghosez, and J.-M. Triscone, *Annu. Rev. Cond. Mat. Phys.* **2**, 141 (2011).

[17] J. Chakhalian, J. W. Freeland, A. J. Millis, C. Panagopoulos, and J. M. Rondinelli, *Rev. Mod. Phys.* **86**, 1189 (2014).

[18] D. Xiao, W. Zhu, Y. Ran, N. Nagaosa, and S. Okamoto, *Nature Commun.* **2**, 596 (2011).

[19] Q.-F. Liang, L.-H. Wu, and X. Hu, *New J. Phys.* **15**, 063031 (2013).

[20] M. Ralle and M. Jansen, *J. Solid State Chem.* **105**, 378 (1993).

[21] J. He, X. Li, P. Lyu, and P. Nachtigall, preprint arXiv:1502.06322.

[22] X.-L. Sheng and B. K. Nikolic, (unpublished).

[23] A. Grutter, F. Wong, E. Arenholz, M. Liberati, A. Vailionis, and Y. Suzuki, *Appl. Phys. Lett.* **96**, 082509 (2010).

[24] S. Agrestini, Z. Hu, C.-Y. Kuo, M. W. Haverkort, K.-T. Ko, N. Hollmann, Q. Liu, E. Pellegrin, M. Valvidares, J. Herrero-Martin, P. Gargiani, P. Gegenwart, M. Schneider, S. Esser, A. Tanaka, A. C. Komarek, and L. H. Tjeng, *Phys. Rev. B* **91**, 075127 (2015).

[25] A. Grutter, F. Wong, E. Arenholz, M. Liberati, A. Vailionis, and Y. Suzuki, *Applied Physics Letters* **96**, 082509 (2010).

[26] A. J. Grutter, F. J. Wong, E. Arenholz, A. Vailionis, and Y. Suzuki, *Phys. Rev. B* **85**, 134429 (2012).

[27] A. J. Grutter, F. J. Wong, C. A. Jenkins, E. Arenholz, A. Vailionis, and Y. Suzuki, *Phys. Rev. B* **88**, 214410 (2013).

[28] X. Ning, Z. Wang, and Z. Zhang, *Journal of Applied Physics* **117**, 093907 (2015).

[29] G. Koster, L. Klein, W. Siemons, G. Rijnders, J. S. Dodge, C.-B. Eom, D. H. Blank, and M. R. Beasley, *Rev. Mod. Phys.* **84**, 253 (2012).

[30] J. P. Perdew, K. Burke, and M. Ernzerhof, *Phys. Rev. Lett.* **77**, 3865 (1996).

[31] G. Kresse and J. Hafner, *Phys. Rev. B* **48**, 13115 (1993).

[32] G. Kresse and J. Furthmller, *Comp. Mat. Sci.* **6**, 15 (1996).

[33] P. Blaha, K. Schwarz, G. Madsen, D. Kvasnicka, and J. Luitz, *An augmented plane wave+ local orbitals program for calculating crystal properties* (2001).

[34] N. Marzari, A. A. Mostofi, J. R. Yates, I. Souza, and D. Vanderbilt, *Rev. Mod. Phys.* **84**, 1419 (2012).

[35] J. Kuneš, R. Arita, P. Wissgott, A. Toschi, H. Ikeda, and K. Held, *Comp. Phys. Comm.* **181**, 1888 (2010).

[36] N. Parragh, A. Toschi, K. Held, and G. Sangiovanni, *Phys. Rev. B* **86**, 155158 (2012).

[37] L. Si, Z. Zhong, J. M. Tomczak, and K. Held, *Phys. Rev. B* **92**, 041108 (2015).

[38] J. Gubernatis, M. Jarrell, R. Silver, and D. Sivia, *Phys. Rev. B* **44**, 6011 (1991).

[39] J. Xia, W. Siemons, G. Koster, M. R. Beasley, and A. Kapitulnik, *Phys. Rev. B* **79**, 140407 (2009).

[40] DMFT overestimates critical temperatures by 20-30% [46] in three dimensions. Of course strictly speaking the Mermin-Wagner theorem prevents long-range ferromagnetic order for a two-dimensional plane. However, because of the exponentially growing correlation length (see e.g. [47]) even well separated bilayers would eventually order in a 2 SRO : 7 STO (111) superstructure at comparable temperatures.

[41] F. Tran and P. Blaha, *Phys. Rev. Lett.* **102**, 226401 (2009).

[42] T. Fukui and Y. Hatsugai, *J. Phys. Soc. Jpn.* **76**, 053702 (2007).

[43] M. L. Sancho, J. L. Sancho, J. L. Sancho, and J. Rubio, *Journal of Physics F: Metal Physics* **15**, 851 (1985).

[44] K. Held, C. Taranto, G. Rohringer, and A. Toschi, *Lecture Notes of the Autumn School 2011 Hands-on LDA+DMFT*, Forschungszentrum Juelich GmbH (publisher)[arXiv:1109.3972] (2011).

[45] C. Cacho, A. Crepaldi, M. Battiatto, J. Braun, F. Cilento, M. Zacchigna, M. C. Richter, O. Heckmann, E. Springate, Y. Liu, S. S. Dhesi, H. Berger, P. Bugnon, K. Held, M. Grioni, H. Ebert, K. Hricovini, J. Minr, and F. Parmigiani, *Phys. Rev. Lett.* **114**, 097401 (2015).

[46] G. Rohringer, A. Toschi, A. Katanin, and K. Held, *Phys. Rev. Lett.* **107**, 256402 (2011).

[47] T. Schäfer, G. Rohringer, O. Gunnarsson, S. Ciuchi, G. Sangiovanni, and A. Toschi, *Phys. Rev. Lett.* **110**, 246405 (2013).